Competing Ferromagnetism and Superconductivity on FeAs Layers in $EuFe_2(As_{0.73}P_{0.27})_2$

Aamir Ahmed,[1] M. Itou,[2] Shenggao Xu,[3] Zhu'an Xu,[3] Guanghan Cao,[3] Y. Sakurai,[2] James Penner-Hahn,[1] and Aniruddha Deb[1,*]

[1]*Department of Chemistry, University of Michigan, Ann Arbor, Michigan 48109, USA*
[2]*Japan Synchrotron Radiation Research Institute (JASRI), SPring-8, Sayo, Hyogo 679-5198, Japan*
[3]*Department of Physics, Zhejiang University, Hangzhou 310027, China*

(Received 2 August 2010; published 11 November 2010)

We have measured the spin-polarized electron momentum density distributions of $EuFe_2(As_{0.73}P_{0.27})_2$ by magnetic Compton scattering (MCS) measurements. For the first time, we show direct evidence of competing ferromagnetism and superconductivity (SC) on FeAs layers in this iron pnictide system. The MCS orbitalwise decomposition of the density distributions reveals that between 16 and 19 K, the spin-polarized Fe-3*d* character is enhanced (as the ferromagnetic character supersedes superconducting character), where the resistivity shows a maximum, reentrant SC-like peak, at 18 K. The spin polarization of the Fe-3*d* orbital, enhanced by ferromagnetic Eu ions, suppresses the SC around 18 K, while at other temperatures the system indeed exhibits SC where the Fe-3*d* spin polarization is suppressed or collapses.

DOI: 10.1103/PhysRevLett.105.207003 PACS numbers: 74.70.Xa, 75.47.Lx, 75.50.−y

Understanding the mechanism of unconventional superconductivity (SC) has been one of the most challenging problems in condensed-matter physics. Since the discovery of SC in iron pnictides by Hosono's group in early 2008 [1], there have been discoveries of high temperature SC in other FeAs layered systems [2–5]. In this developing field of Fe-pnictide SC attention is drawn in comparison to cuprate high temperature superconductors, containing partially filled *d*-electron spins, present in the parent phase that are antiferromagnetically (AFM) aligned similar to pnictides and SC arises when magnetism is suppressed. Like the cuprates, the Fe-based superconductors [6,7] are derived from either electron [1,8–10] or hole [11] doping in a parent compound, characterized by an antiferromagnetic spin-density-wave (SDW) transition associated with the FeAs layers [2,12].

Among the parent systems in the ferroarsenide family, $EuFe_2As_2$ exhibits a SDW transition around $T_0 = 190$ K related to the Fe_2As_2 layers, at $T_N = 20$ K the magnetic moments of the localized Eu^{2+} moments order [13–15] in a so-called *A*-type antiferromagnetic structure [16]. A strong coupling between the magnetism of Eu^{2+} ions and conduction electrons is proposed to destroy the SC [17]. Intriguingly, recently in this ferroarsenide family, the first ferromagnetic superconductor was reported with the partial substitution of As with *P* in the parent system of $EuFe_2As_2$ [18]. The phosphorus doping leads to a coexistence of superconductivity and ferromagnetism.

The antagonistic nature between SC and FM has long been recognized. Conventionally, SC and FM exclude each other because FM implies the existence of a strong permanent magnetic field while SC expels the magnetic field (Meissner effect). The internal magnetic field generated by ferromagnetic ions destroys the superconductivity due to orbital [19] and paramagnetic limiting (for systems with spin singlet SC) [20]. In this Letter, for the first time, we demonstrate how superconductivity and ferromagnetism compete with each other in the FeAs layers. This is important because the competing (i.e., the rise and the collapse) Fe-3*d* spin contribution is responsible for reentrant SC below 18 K. Though the previous study [18] on the similar system predicts the ferromagnetic alignment of the Eu^{2+} spin at 18 K, this Letter shows direct evidence that SC and FM compete with each other in FeAs layers.

Polycrystalline samples of $EuFe_2(As_{0.73}P_{0.27})_2$ were synthesized by solid state reaction as reported earlier and the phase purity of the sample was checked by powder x-ray diffraction (XRD) [18]. Figure 1 shows the temperature dependence of resistivity in this system, where the resistivity drops sharply below $T = 26$ K, the superconducting transition. The inset of Fig. 1 shows a small resistivity peak at $T = 18$ K, suggesting loss of superconductivity, which coincides with the ferromagnetic ordering of the Eu^{2+} moments [18], and the reentrance of superconductivity below 16 K. This peculiar loss and reentrance of superconductivity arises from the competing superconductivity and ferromagnetic character in the FeAs layer (to be shown below).

Magnetic Compton scattering (MCS) is a valuable tool for investigating the spin-polarized orbitals in ferro- or ferrimagnetic materials [21]. The Compton profile (CP), $J(p_z)$, is related to the double-integrated ground-state electron momentum density as

$$J(p_z) = \iint \left(\sum_i |\rho_{i\uparrow}(\mathbf{p})|^2 + \sum_i |\rho_{i\downarrow}(\mathbf{p})|^2 \right) dp_x dp_y \qquad (1)$$

and magnetic Compton profile (MCP), $J_{\mathrm{mag}}(p_z)$, is defined as

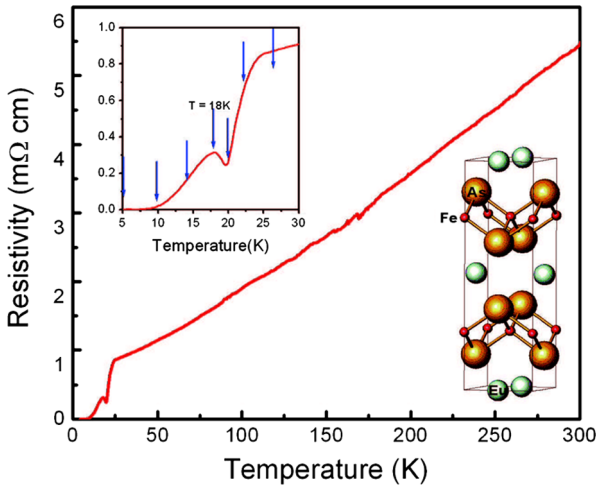

FIG. 1 (color online). Temperature dependence of resistivity, the inset on the left shows an expanded plot of the resistivity, the blue arrows show the temperatures where we have taken the MCP measurements; the inset on the lower right shows the crystal structure for the parent 122 superconductor system $EuFe_2As_2$.

$$J_{\mathrm{mag}}(p_z) = \iint \Big(\sum_i |\rho_{i\uparrow}(\mathbf{p})|^2 - \sum_i |\rho_{i\downarrow}(\mathbf{p})|^2 \Big) dp_x dp_y \quad (2)$$

where, $\rho_{i\uparrow}(\mathbf{p})$ is the up-spin electron momentum density, $\rho_{i\downarrow}(\mathbf{p})$ the down-spin electron momentum density, and i runs through the occupied electronic states. The z component, p_z, of the electron momentum $\mathbf{p} = (p_x, p_y, p_z)$ is taken along the direction of the scattering vector. Using circularly polarized x rays, the MCP is obtained experimentally by taking the difference of the Compton scattering intensities with the reversal of the magnetization direction. The flipping ratio R_{sample}, which is proportional to the net spin moment is defined as

$$R_{\mathrm{sample}} = \frac{I^+ - I^-}{I^+ + I^-} \propto \frac{\int J_{\mathrm{mag}}(p_z) dp_z}{\int J(p_z) dp_z}, \quad (3)$$

where I^+ and I^- are the intensities of Compton-scattered x rays with the different magnetization directions. The spin moment of the sample, μ_{sample}, from the MCP experiment is obtained by comparing the R_{Fe} measured for Fe under the sample experimental conditions as

$$\mu_{\mathrm{sample}} = \mu_{\mathrm{Fe}} \Big(\frac{M_{\mathrm{sample}} R_{\mathrm{sample}}}{M_{\mathrm{Fe}} R_{\mathrm{Fe}}} \Big), \quad (4)$$

where M_{sample} and M_{Fe} are the effective number of electrons contributing to the total inelastic scattering for the sample and Fe. Since the spin moment for Fe ($2.1\mu_B$) [22] is well known the spin moment for the sample can be obtained accurately.

MCP experiments were performed at the BL08W beam line of SPring-8 Japan. The measurements were performed at different temperatures which were chosen based on the resistivity measurements in Fig. 1. Circularly polarized x rays were monochromatized to 175 keV and incident on the sample, with a scattering angle of 178.5°, and analyzed by a

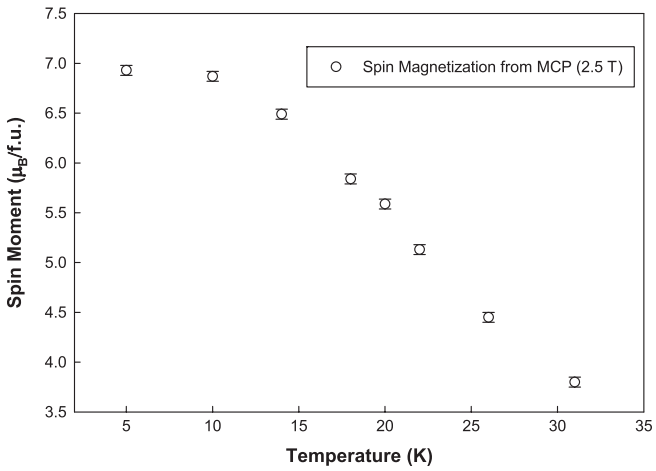

FIG. 2. Temperature dependent experimental spin moments per formula unit (μ_B) observed with a magnetic field of 2.5 T.

10-element Ge solid state detector. To reverse the direction of magnetization, an applied external magnetic field of ± 2.5 T was alternatively applied on the sample. The MCP's extracted were then corrected for sample absorption and scattering cross section [23]. Each MCP was normalized by the magnetic electrons obtained by comparison with Fe as discussed earlier [Eq. (4)]. The total spin moment obtained from the MCP data is shown in Fig. 2.

The differences in MCPs between two different temperatures are shown in Fig. 3. From the difference MCPs (Fig. 3), instantly, two interesting changes can be observed. For the 14–18 K MCP profile, there is a shape change (represents a triangle shape with a sharp vertex [labeled A] at $p_z = 0$ a.u., while for the others the shape is flat at $p_z = 0$ a.u.) with respect to the others. For the 18–20 K, the MCP profile shows a large dip [labeled B] at $p_z = 0$ a.u.; hence, we can conclude that the "distinct" changes for both of these temperature difference profiles (compared to the others), are arising from the $T = 18$ K MCP profile, where the system loses superconductivity as seen from the resistivity measurements in Fig. 1.

In order to understand the origin of this observed shape change in the temperature difference MCPs we calculated the total and orbitalwise MCPs using KKR-CPA calculations [24]. In the present calculations, the l_{max} for the major component of the wave function was restricted to 4 for Eu, 3 for Fe, As, and P. Individual orbitalwise contributions to the total MCP were calculated for Eu-5f; Fe-3d, 4s and 4p; As-4p; and P-3p. Using these calculated KKR-CPA orbitalwise MCPs we then fitted the experimental temperature dependent MCPs (shown in insets of Fig. 4). The results of the theoretical temperature difference MCPs to the experimental difference are shown in Fig. 3. The KKR-CPA orbitalwise temperature difference (Fig. 3) fit results shows similar shape change for the 14–18 K difference profile, and also represent the large dip at $p_z = 0$ for the 18–20 K difference MCP, as observed experimentally.

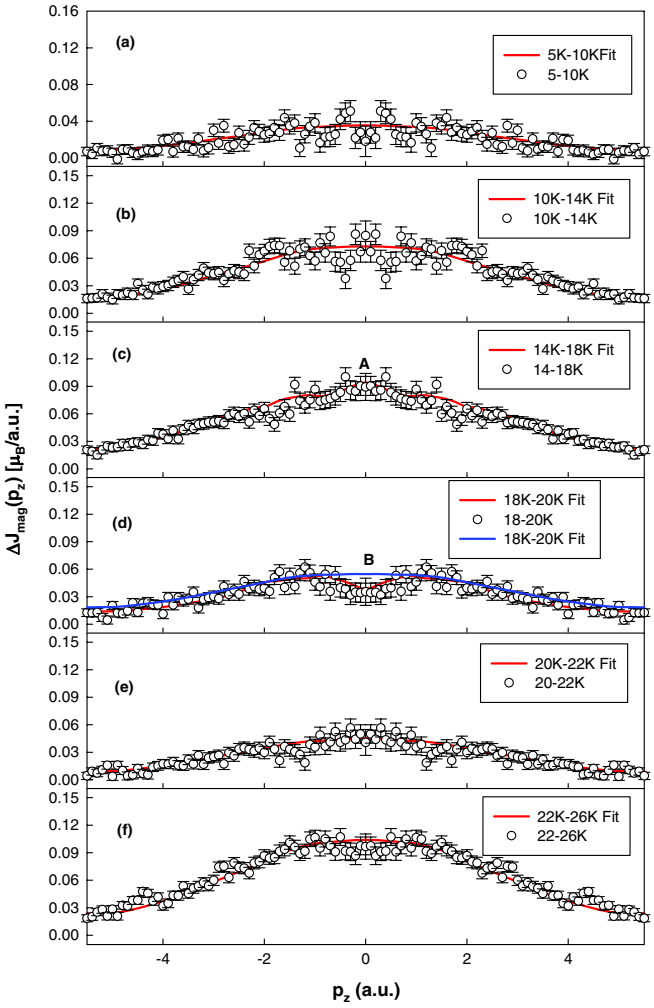

FIG. 3 (color online). Temperature difference MCP under an applied field of 2.5 T: (a) 5–10 K, (b) 10–14 K, (c) 14–18 K, (d) 18–20 K, (e) 20–22 K, and (f) 22–26 K. The experimental data are shown as circles and the KKR-CPA fit are shown as solid (red) lines. The label A in (c) show the sharp vertex, representing the change in shape; while label B in (d) shows the large dip at $p_z = 0$ a.u. The solid (blue, online) line in (d) shows the best fit obtained by constraining Fe 3d to 0.05μ_B (for details see text).

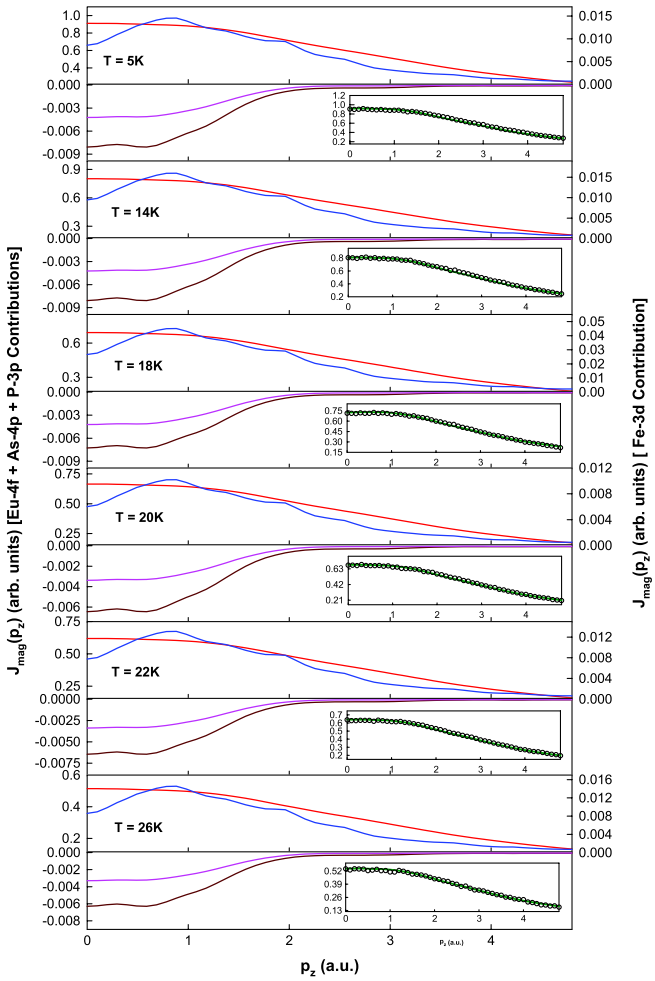

FIG. 4 (color online). Individual orbitalwise contributions of Eu-4f, Fe-3d, As-4p, and P-3p used for the fit to the experimental data (shown in the inset), at different temperatures. The upper panel shows the contributions from Eu-4f (red, online) and Fe-3d (blue, online); the lower panel shows the contribution from As-4p (brown, online) and P-3p (purple, online), respectively. The inset shows the fit to the experimental MCPs at different temperatures using these KKR-CPA orbitalwise theoretical MCPs.

Importantly, the fit produces very good representation of the experimental difference MCPs, by only considering the Eu-5f, Fe-3d, As-4p, and P-3p contributions, hence the Fe-4s and 4p were finally not included in the fit as it did not improve the fit significantly. Figure 4 shows the KKR-CPA orbitalwise contributions that are used in the temperature dependent MCPs to fit the experimental MCPs (as shown in insets of Fig. 4). Comparing these, we can see that as temperature decreases the Eu-4f contribution increases, but the most striking feature is the Fe-3d contribution at 18 K, where the Fe-3d contribution increases sharply (approximately 4 times around $p_z = 0.9$ a.u.) with respect to the other temperatures, while the contributions from the As-4p and P-3p remains almost the same for all the temperatures. Important to note, that the As-4p and P-3p are aligned antiparallel with respect to Eu-4f and Fe-3d.

In order to understand further quantitatively, we find the area under each of these individual orbitalwise (Eu-4f, Fe-3d, As-4p, and P-3p) MCP profiles shown in Fig. 4, as the area equals the number of magnetic or unpaired electrons. The results are shown in Fig. 5, where we see that Eu-4f dominates the spin moment for all temperatures and the Fe-3d contribution is lower and accounts to about 1.0% $\sim$ 5% of the Eu-4f moment, where the highest 5% contribution is at 18 K. In order to demonstrate that the highest Fe-3d contribution is essential at 18 K [for the best fit shown by the pink solid line, online, in Fig. 3(d)], a fit (solid blue line, online) is also shown where we have constrained the Fe-3d contribution to 0.05μ_B, which provides a vivid demonstration on the point that one cannot reproduce the minimum identified as "B" unless there is a substantial change in the Fe-3d contribution at 18 K.

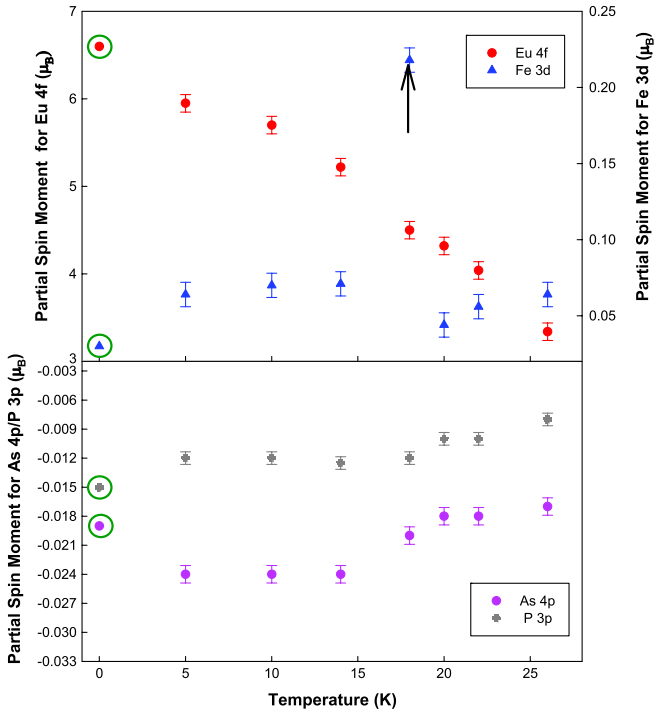

FIG. 5 (color online). Temperature dependent orbitalwise partial spin moment contributions. The upper panel shows the contributions from Eu-4f and Fe-3d orbitals; the lower panel shows the contributions from As-4p and P-3p orbitals. The points at $T = 0$ K are marked with circles, representing the values of the individual orbital contribution from KKR-CPA calculations.

These observations clearly exhibit the competing ferromagnetism and superconductivity in the FeAs layers. The resistivity peak at 18 K which implies loss of SC, the MCP results explains that the internal magnetic field produced by Eu-4f orbital FM ordering along with the Fe-3d orbital contribution (maximum at 18 K) exceeds the SC upper critical field in a narrow temperature range (from around $16 \sim 19$ K). Hence in this temperature range, due to the competing SC and ferromagnetic character, the ferromagnetic character supersedes SC character, and we see a maximum in the resistivity data and also a maximum in the Fe-3d character (at 18 K). In the case of nonzero, but very small resistivity (Fig. 1), one expects "spontaneous vortex" (generated by Eu-FM), which could cause dissipation when the sample carries electric current. This means that except for the narrow temperature window between 16 and 19 K (where the Fe-3d orbitals contribution increases 4 times, about 5% of the Eu-4f moments), the sample indeed exhibits SC, where Fe moment collapses (Fe-3d orbitals, about 1% of the Eu-4f moment).

Around 18 K the sample becomes "normal" because of the suppression of SC by a combination of magnetic effect from Eu-4f and Fe-3d contributions. Important to remember that the SC is derived from the AFM parent compound $EuFe_2As_2$ where Fe carries a moment of about $1\mu_B$. So, as one of the possibilities, we can conclude that the Eu-FM induce Fe moments when SC is suppressed that is what we see from our MCP data a 4 times increase of the Fe-3d contribution.

In summary, the results clearly show the competing SC and FM interplay in the FeAs layers for the system and the ferromagnetic character is dominated by the Eu layers. The Eu-4f orbital FM ordering along with the Fe-3d orbital contribution exceeds the SC upper critical field for $T = 16$–19 K; hence in this temperature range due to the competing SC and FM character, the FM character supersedes SC character, and a reentrant superconductivity character is observed in the resistivity data. At 18 K, SC is suppressed by a combination of magnetic effect of the Fe-3d and Eu-4f contribution, while except at 18 K we see that the Fe moment collapses.

We would like to thank Dr. Sergey Mankovsky for the valuable discussions. This work was performed with the approval of the JASRI (Proposal No. 2010A1084).

*debani@umich.edu

[1] Y. Kamihara *et al.*, J. Am. Chem. Soc. **130**, 3296 (2008).
[2] J. Dong *et al.*, Europhys. Lett. **83**, 27006 (2008).
[3] G. F. Chen *et al.*, Phys. Rev. Lett. **100**, 247002 (2008).
[4] Zhi-An Ren *et al.*, Europhys. Lett. **83**, 17 002 (2008).
[5] X. H. Chen *et al.*, Nature (London) **453**, 761 (2008).
[6] S. A. Kivelson *et al.*, Nature Mater. **7**, 927 (2008).
[7] C. K. Xu *et al.*, Nature Phys. **4**, 898 (2008).
[8] A. S. Sefat *et al.*, Phys. Rev. Lett. **101**, 117004 (2008).
[9] A. Leithe-Jasper *et al.*, Phys. Rev. Lett. **101**, 207004 (2008).
[10] L. J. Li *et al.*, New J. Phys. **11**, 025008 (2009).
[11] M. Rotter, M. Tegel, and D. Johrendt, Phys. Rev. Lett. **101**, 107006 (2008).
[12] Clarina de la Cruz *et al.*, Nature (London) **453**, 899 (2008).
[13] H. Raffius *et al.*, J. Phys. Chem. Solids **54**, 135 (1993).
[14] H. S. Jeevan *et al.*, Phys. Rev. B **78**, 052502 (2008).
[15] Z. Ren *et al.*, Phys. Rev. B **78**, 052501 (2008).
[16] S. Jiang *et al.*, New J. Phys. **11**, 025007 (2009).
[17] H. S. Jeevan *et al.*, Phys. Rev. B **78**, 052502 (2008).
[18] Zhi Ren *et al.*, Phys. Rev. Lett. **102**, 137002 (2009).
[19] V. L. Ginzburg, Sov. Phys. JETP **4**, 153 (1957).
[20] D. Saint-James, G. Sarma, and E. J. Thomas, *Type II Superconductivity* (Pergamon, New York, 1969).
[21] *X-Ray Compton Scattering*, edited by M. J. Cooper *et al.* (Oxford University Press, Oxford, 2004); A. Koizumi *et al.*, Phys. Rev. Lett. **86**, 5589 (2001); A. Deb *et al.*, Phys. Rev. B **63**, 064409 (2001); B. Barbiellini *et al.*, Phys. Rev. Lett. **102**, 206402 (2009).
[22] J. E. McCarthy *et al.*, J. Synchrotron Radiat. **4**, 102 (1997).
[23] N. Sakai, J. Phys. Soc. Jpn. **56**, 2477 (1987).
[24] The Munich SPR-KKR package, version 5.4; H. Ebert *et al.*, http://olymp.cup.uni-muenchen.de/ak/ebert/SPRKKR.